Effects of plastic hinges on partial interaction behaviour of bolted side-plated beams

W.H. Siu[1], R.K.L. Su[2*]

[1] PhD candidate

[2] Assistant Professor

*Corresponding author

Address: Department of Civil Engineering, The University of Hong Kong, Pokfulam Road, Hong Kong, PRC

Fax number: (852) 2559 5337

E-mail address: klsu@hkucc.hku.hk

Abstract

Slips of mechanical connectors in steel plate reinforced concrete (RC) structures can significantly affect the load-carrying capacity of the structures. The difference in deformation between the steel plate and the reinforced concrete counterpart is known as partial interaction. In this study, the flexural behaviour of bolted side-plated (BSP) reinforced concrete beams was investigated experimentally. Two new deformation-based parameters, namely the strain factor and curvature factor, were introduced to quantify the degree of partial interaction between the RC beam and the steel plates. The experimental results revealed that the degree of partial interaction between RC beams and steel plates could be reduced by as much as 50% when the BSP beam proceeded from linear to non-linear stage in which plastic hinges have formed in critical sections. Consequently, the load-carrying capacity was reduced by up to 30% of the theoretical additional strength provided by the bolt-plate system, which is more than double the allowance proposed previously in the literature. The under-estimation of the effect of partial interaction in composite structures can result in unsafe design.

Keywords

Bolts, reinforced concrete beams, curvature, non-linear, plate, slip strain

1. Introduction

Steel often combines with reinforced concrete (RC) to form a composite system such that the high performance of steel in tension and concrete in compression can be fully utilized. Some common composite systems include steel girders with a concrete slab on top, hollow steel columns in-filled with concrete, composite slabs formed by steel decking with concrete slabs and bolted side-plated (BSP) beams, where steel plates are anchored on the side faces of RC beams with bolts.

In BSP beams, since bolts are used to anchor steel plates on the RC beam core, slip between the RC beam and the steel plates is required in order to mobilize anchor bolts and forces can be transferred to the steel plates. Because of such relative slip, the deformation of the steel plates is reduced and is less than the deformation of the RC beam. The difference in deformation is known as partial interaction.

A number of studies have been carried out to investigate the flexural behaviour of BSP beams [1-4]. These studies revealed that the partial interaction in BSP beams occur in both longitudinal and transverse directions, and significantly lower the strength of BSP beams even when sufficient strength of bolts are provided. To prevent over-estimation of flexural strength, the effect of partial interaction has to be considered in the analysis of BSP beams. Mathematical models have been developed [1,2] to describe the partial interaction in BSP beams. However, the elastic assumption was made of RC and steel plates in these studies and the inelastic behaviour of BSP beams have not been investigated.

In this study, four-point bending tests on simply-supported beam specimens were carried out to investigate the inelastic behaviour of BSP beams in particular, the influence of plastic hinges at critical sections. Various strengthening schemes using different bolt-plate arrangements were tested. Two new deformation-based parameters,

strain and curvature factors, were defined and used to quantify the degree of partial interaction of steel plate strengthened beams. The influences of slips between the RC beam and the steel plates and slip strain accumulation at plastic hinges were investigated in detail. A special device consisting of a rhombic arrangement of linear variable direct transducers (LVDTs) was developed to measure the slip between the RC beam and the steel plates at different locations of the beam.

2. Experimental Program

2.1 Test Setup

A four-point bending test setup, as shown in Fig.1, was adopted. The beam specimens were simply-supported with a clear span of 3600 mm. Load was applied by a 1000 kN hydraulic jack in the vertical direction, divided into two equal point loads and exerted symmetrically 600 mm on either side from the mid-span onto the specimen through a transfer beam. With this arrangement, a pure bending zone with constant moment was created so that the flexural behaviour under pure bending could be studied.

2.2 Specimen Details

Five specimens were fabricated and tested. The dimensions of the RC beams were 225×350×4000 mm (width×depth×length). The beams were under-reinforced by 3T16 longitudinal reinforcements. Transverse reinforcement of T10-150 was applied throughout the span of the beams. This amount of reinforcement would be sufficient to ensure that the specimens would fail in flexure in both the un-strengthened and strengthened cases.

Specimen NBNP is the control specimen without any strengthening measures. The other specimens are plate strengthened with four different bolt-plate combinations

including ‘Strong-Bolt Strong-Plate’ (SBSP), ‘Weak-Bolt Strong-Plate’ (WBSP), ‘Weak-Bolt Weak-Plate’ (WBWP) and ‘Strong-Bolt Weak-Plate’ (SBWP). The bolt-plate arrangements, having been identified as the major parameter affecting the structural behaviour of BSP beams, were properly selected so that the effect of plastic hinges on all bolt-plate combinations could be covered.

The strengthening details are summarized in Table 1 and illustrated in Fig. 2. Mild steel plates of two different plate sizes, 6×150 mm deep and 6×75 mm deep, on both side faces of specimens were chosen to be the ‘Strong’ and ‘Weak’ plate arrangements, respectively, equivalent to 2.3% and 1.1% of the gross sectional area of concrete. The centroidal axes of the steel plates in all strengthened specimens were set at 250 mm from the top of the beam. By setting the centroidal axis to a level on the tension side and relatively further away from the neutral axis, the buckling of steel plates, which is out of the scope of this study, is prevented.

In this study, the degree of shear connection η [4] is used to consider whether a bolt arrangement is ‘Strong’ or ‘Weak’. The degree of shear connection is defined as

$$\eta = \frac{P_b}{F_{p,fsc,fi}}, \tag{1}$$

where P_b is the total ultimate strength of bolts on a shear span and $F_{p,fsc,fi}$ is the plate force at peak load in the full interaction case.

To estimate the degree of shear connection of specimens, the plate force at peak load under full interaction is required. Therefore, the full interaction analysis, which assumes that the strain profile of the RC beam and the steel plate coincides, has been carried out. The analysis adopted elastic-plastic models for steel plates and reinforcements, and a non-linear model for concrete, which is described in Appendix B. Incremental curvatures were applied to the section in each step. The neutral axis

level was adjusted until horizontal force equilibrium was reached. With the strain profile fixed, the moment of the section can be solved by taking the moment about the neutral axis, while the plate force can be solved accordingly.

The degrees of shear connection of the specimens are given in Table 1. The degrees of shear connection of Specimens SBSP and SBWP are 1.00 and 1.26, respectively, implying that sufficient bolts have been provided for full shear connection and the bolt arrangement is 'Strong'. Conversely, the degrees of shear connection of Specimens WBSP and WBWP are 0.38 and 0.75, respectively; signifying that these specimens have 'Weak' bolt arrangements.

2.3 Material properties

A concrete mix containing maximum coarse aggregates of 10mm together with target mean cube strength of 30 MPa at 28 days after casting was designed for the specimens. Concrete cube compressive tests were carried out on the test days to obtain the compressive strength of cubes. The average concrete compressive strength of cubes for the control specimen is 35.2 MPa and for the BSP specimens are given in Table 1.

High yield steel reinforcement with characteristic yield strength of 460 MPa was used in this study. The yield strength, yield strain and Young's modulus of the reinforcements and steel plates are summarized in Table 2.

ϕ12 HAS-E anchor rods [6] provided by the Hilti Corporation were used as the mechanical connectors of all specimens. The HAS-E rod was in Grade 5.8 steel, with a minimum 5μm galvanized surface. Dynamic sets, instead of ordinary washers and nuts, were used in this study. A spherical washer, an injection washer and an ordinary nut were included in a dynamic set, as illustrated in Fig. 3. By using the dynamic sets

washers, the gaps between connecting components and the bolt shaft as well as between the anchoring steel plates and the bolt shafts were fully filled up with epoxy. Hence, majority of loads were transferred through bearing instead of friction and all components were in contact once loading was applied; the undesirable slips can be avoided. Two bolt shear tests were carried out to measure the load-deformation responses of anchor bolts. The results of the shear tests are plotted in Fig. 4. Linear responses were observed for both specimens up to 40kN. Then the stiffness of bolts dropped gradually up to the peak load. The average ultimate strength of bolts was 76kN. A bi-linear relationship, as presented in Fig. 4, was used to simplify the non-linear load-deformation responses.

2.4 Instrumentations

2.4.1 Strain gauge arrangements

Strain gauges were attached on the steel plates, the longitudinal reinforcements to measure the internal strains, which were then used to determine the internal stress distributions in specimens. These strain gauges were installed along the direction of the beam span at five different sections. Three sections were within the constant moment zone and two at the middle of the left and right shear spans, as illustrated in Fig. 5. Three sets of strain gauges were installed in the constant moment zone to measure the average response of the zone. The measured data may be affected by localized effects such as cracking of concrete and buckling of compression reinforcement if only one set of measurements is used. With the use of three sets of measurements, the behaviour of the zone can be better represented.

2.4.2 LVDT and LDT arrangements

Linear variable direct transducers and linear displacement transducers (LDTs) were installed, as illustrated in Fig. 6. The LVDTs other than those in the constant moment zone were installed and located along the centreline of the section. At the constant moment zone, installation along the centreline is not possible, as the space was blocked by the transfer beam. In this case, pairs of LDTs, as shown in Fig. 6, were installed and the average of the readings was used to represent the vertical displacement of the beam section.

2.4.3 Rhombic arrangements of LVDTs

One of the primary objectives of this experimental study is to measure the non-linear slip responses between the RC beam and the steel plates. The major difficulty in measuring the slip is that the surface of the RC beam is covered by the steel plate at the locations where the slips are of interest. Furthermore, slips can be in all directions: longitudinal, transverse and rotational. To overcome the above difficulties, a new rhombic arrangement of LVDTs, which is able to measure the slips between two target planes 'AD' and 'EF' of the RC beam and the steel plate, respectively, was invented to trace the slip responses (see Fig. 7).

Fig. 7(a) shows the instrumentation of a LVDT to measure the distance between two reference points. As the reference points (A, B, C and D) moved relative to each other, a change in the length of the extensible rod would be recorded by the LVDTs installed adjacent to it. With hinges installed, any rotation of the rod could be accommodated.

The rhombic arrangement of LVDTs is illustrated in Fig. 7(b). Four reference points, two on the RC beam and the other two on the steel plate, were used to define the transverse target planes 'AD' of the RC beam and 'EF' of the steel plate. The

reference points of the target plane ‘AD’ of the RC beam were located above and below the steel plate so that the reference points were not covered up by the steel plate. The reference points B and C of the target plane ‘EF’ of the steel plate were set on the left and right hand sides of the target plane. As the reference points B and C were not on the target plane, a metal strip was used to extend the target plane to the reference points. The metal strip was anchored on the target plane with two screws so that it would move rigidly with the target plane ‘EF’ under both translational and rotational movements. To ensure accurate measurements, the metal strip was offset from the steel plate so that the strip and the plate were not in contact, except at the anchorage points.

By measuring the relative distances between reference points, the slip between the target planes could be evaluated. The details can be found in Appendix A. Rhombic arrangements of LVDTs were installed on the specimens to measure the slip responses at various locations, as illustrated in Fig. 6. The same rhombic arrangements of LVDTs were installed at the back face of the beams. The locations of LVDTs for Specimen SBWP were slightly different from the other specimens in order to prevent the arrangement from clashing with the screw heads.

2.5 Loading history

In each test, the specimen was first incrementally loaded to 50% of the ultimate capacity of the beam, as estimated by full interaction section analyses. After that, the loading process was changed to a displacement-controlled mode in which incremental displacements were applied. The loading process was terminated when the applied loading was dropped to 85% of the peak load, or any of the two bolts in the specimen were fractured.

3. Experimental Results

3.1 General

The ultimate strengths of the five specimens are presented in Table 3. The ultimate strength of BSP specimens was increased by 32kN to 60kN, equivalent to the increase of 32% to 59% to the ultimate capacity of the unstrengthened specimen NBNP. Specimen SBSP, strengthened by both 'strong bolt' and 'strong plate', was the strongest among the specimens, followed by specimens WBSP and SBWP. Specimen WBWP, being the weakest among the four specimens, has 32% additional strength comparing to the unstrengthened case.

The failure modes of specimens are summarized in Table 3 and displayed in Fig. 8. Two different failure modes were observed for 'Strong' bolt and 'Weak' bolt arranged specimens. Specimens SBSP and SBWP, with sufficient bolts installed, failed in concrete crushing after the yielding of the bottom reinforcement. Specimens WBSP and WBWP, with insufficient bolts installed, failed in bolt fracture. In both specimens, the bolts closest to the supports fractured leading to an abrupt failure.

3.2 Load-deflection response

The moment-deflection responses at the mid-span of the five specimens are plotted in Fig. 9. As shown in the figure, the responses of 'Strong' bolt and 'Weak' bolt arranged specimens are quite different. 'Strong' bolt arranged specimens WBSP and WBWP responded linearly when initial load was applied. After the linear region, the stiffness dropped gradually and deformation continued until the bolts fractured suddenly; no descending branch was observed.

'Weak' bolt arranged specimens SBSP and SBWP also responded linearly at the initial loading stage. The stiffness dropped gradually afterwards but the specimens

were still able to take up further loadings up to the peak load. After reaching the peak load, a gradual descending branch was observed due to crushing of concrete until failure occurred.

3.3 Longitudinal slip responses

The full range longitudinal slip responses of all strengthened specimens were captured by the rhombic arrangement LVDTs and are plotted in Fig. 10 and the maximum slip at various locations of specimens are summarized in Table 4. The responses between 'Strong' bolt (Specimen SBSP and Specimen SBWP) and 'Weak' bolt (Specimen WBSP and Specimen WBWP) arranged specimens are significantly different. For the 'Strong' bolt arranged specimens, the slips were very small (<0.2mm) when initial loading was applied, as most of the force transferred to the steel plates was taken up by the friction between the RC beam and the steel plates. The bolts were mobilized as the applied load increased, and the relationship between the longitudinal slips and the mid-span deflections was approximately linear at various locations along beam span until the mid-span deflections reached the deflections corresponding to the peak load (i.e., 35 mm and 44 mm for Specimens SBSP and SBWP, respectively). In the post-peak stage, the slips increased more slowly than in the pre-peak stage, until failure occurred.

Both 'Weak' bolt specimens (Specimens WBSP and WBWP) failed in bolt fracture. The initial responses of these two specimens are similar to 'Strong' bolt arranged specimens, as friction existed in all Specimens. After the bolts were deformed and mobilized, slips gradually developed between the RC beam and the steel plates. As the beam approached failure, the rate of longitudinal slip also increased gradually. It should be noted that the rate described herein is relative to the deflection of the mid-

span. A higher rate in increase of slip suggests that the ductility demand for bolts may be greater than the ductility demand for the beam, and should be taken into account when choosing bolts in practical designs. To prevent premature failure of bolts, ductility of bolts should be considered carefully if a partial-shear-connection design is carried out.

4. Result analysis

4.1 Reduction of moment resistance due to partial shear connection and interaction

The moment resistance of any mechanically-connected BSP beam is lower than that predicted from full-shear-connection full-interaction analysis due to the existence of partial interaction and/or partial shear connection. All specimens were affected by the effects of partial interaction, while both full-shear-connection and partial-shear-connection cases have been covered in this study. Serving as a reference, full-shear-connection full-interaction analysis has been carried out, as described in Section 2.2, so that the theoretical increase in the moment capacity under a full-interaction full-shear-connection assumption could be solved. The additional moment ΔM_u provided by various bolt-plate systems are listed in Table 5 and compared with the theoretical additional moment obtained in the full-shear-connection full-interaction analysis $\Delta M_{u,fsc,fi}$. The specimens showed 25% to 51% reduction in additional moment resistance as compared with the full-shear-connection full-interaction case.

Specimens WBSP and WBWP are subject to greater additional moment reductions of 51% and 44%, respectively. This is because both partial shear connection (insufficient shear strength of the connecting media) and partial interaction (slip of the connecting media) existed, as the degrees of shear connections of the two specimens are less than one (see Table 5).

Full shear connection existed in Specimens SBSP and SBWP, as the degrees of shear connections are 1.00 and 1.26, respectively. Therefore, the reduction in additional moment resistance was solely due to the effect of partial shear interaction. According to Table 5, the reductions in additional moment resistance for these two specimens are 38% and 25%, respectively. Although full shear connections were provided in both cases, the reductions in additional moment resistance are still significant and are much higher than the 15% reduction, as previously suggested [4] for incorporating the effects of partial interaction. Apparently, this suggestion cannot fully account for the effect of partial shear interaction on the reduction of moment resistance of BSP beams.

4.2 Partial interaction response

In this study, the partial interaction at the peak moment section is quantified by two factors, the strain factor and the curvature factor [9, 10] of the critical section (section with the largest moment), as illustrated in Fig. 11. These two factors quantified the ratio of cross-sectional deformation between the RC beam and the steel plates and are appropriate for describing the partial interaction responses, which are fully controlled by the displacement compatibility of the RC beam, the steel plate and the anchoring bolts. The longitudinal partial interaction is quantified by the strain factor of the critical section, which is defined mathematically as

$$\alpha_{\varepsilon} = \frac{\varepsilon_{p,h_p}}{\varepsilon_{c,h_p}} \tag{2}$$

where ε_{p,h_p} and ε_{c,h_p} are the longitudinal strains of the steel plates and the RC beam at the centroidal level of the steel plate of the corresponding section, respectively. When the strain factor of the critical section is equal to 1, full longitudinal partial interaction exists and the longitudinal strain at the plate's centroidal level is the same as that of

the adjacent concrete. In this case, the maximum plate force is induced in the steel plates. When partial interaction exists, the strain factor is smaller than 1 and the longitudinal strain is reduced to $\alpha_\varepsilon \varepsilon_{c,h_p}$. In the extreme case, the strain factor is zero and no net axial force is induced in the steel plates.

Considering the compatibility between the RC beam, the steel plates and slip at the critical section, as shown in Fig. 11, the strain in concrete, and hence the strain factor, can be expressed in terms of the strain in the steel plates and the slip strains at the centroidal level of the steel plates as

$$\varepsilon_{c,h_p} = \varepsilon_{p,h_p} + \varepsilon_{slip,h_p}, \tag{3}$$

$$\alpha_\varepsilon = \frac{\varepsilon_{p,h_p}}{\varepsilon_{p,h_p} + \varepsilon_{slip,h_p}}. \tag{4}$$

On the other hand, the curvature factor of the critical section is used to quantify the transverse interaction between the RC beam and the steel plate and is defined as

$$\alpha_\phi = \frac{\phi_p}{\phi_c} \tag{5}$$

where ϕ_p and ϕ_c are the curvatures of the steel plates and the RC beam of the corresponding section, respectively. Full transverse interaction is present when the curvature is equal to 1 and the curvatures of the RC beam and the steel plates are the same. When partial interaction exists, the curvature of the steel plates is smaller than that of the RC beam and the curvature factor is between 0 and 1. When the curvature factor is 0, the beam exhibits no transverse interaction.

4.2.1 Variation of strain factor of the critical section

The longitudinal strains of the steel plate at its centroidal level (ε_{p,h_p}) of the critical section were measured directly by the strain gauges attached at the centroidal level of

plate h_p, as shown in Fig. 5. Assuming plane sections remain plane after bending, the longitudinal strains of RC at the centroidal level of the plate (ε_{c,h_p}) could be expressed mathematically as

$$\varepsilon_{c,h_p} = \varepsilon_{c,\text{top gauge}} + \phi_c (h_p - d_{c,\text{top gauge}}) \quad (6)$$

where $\varepsilon_{c,\text{top gauge}}$ is the average of the strain gauge readings from the top reinforcement in the constant moment zone, ϕ_c is the average curvature of concrete in the constant moment zone as estimated by LVDTs [5], h_p is the depth of the centroidal level of the steel plate, and $d_{c,\text{top gauge}}$ is the depth of the top reinforcement where the strain gauge is attached.

Using Equations (2) and (6), the strain factor can be solved. The variation of the strain factor against the mid-span deflection of the RC beam in the constant moment zone is plotted in Fig. 12. The instants when the average readings of strain gauges attached on the bottom reinforcement of beams in the constant moment zone reached the yield strain of reinforcement obtained from the material tests (i.e. yielding of the bottom reinforcement) are also pointed out in Fig. 12.

Prior to yielding of the bottom reinforcement, a gradual descending trend for the strain factor of all specimens is observed. The gradual drop in strain factor is due to the fact that instead of the assumed bi-linear relationship, the stiffness of bolts and hence the stiffness of the connecting media reduces gradually once loading has been applied. This results in a drop in both the strain factor of the critical section and the longitudinal partial interaction of the beam.

As shown in Fig. 12, the strain factor decreased more significantly as a plastic hinge began to form in the critical section of the RC beam. The strain factor at the critical section of specimens at the ultimate limit state was reduced to between 44% and 53%

of the value when the bottom reinforcement yielded. One of the possible reasons for such reduction in partial interaction is the formation of plastic hinges at the critical section of the beam. When a plastic hinge forms in the critical section of the RC beam, a large curvature is accumulated in the plastic hinge, as the beam is subject to further deformation due to the low flexural stiffness of the hinge. This results in a rapid increase of concrete strain at the centroidal level of the steel plate. As the concrete strain is the denominator of the strain factor (see Equation 2), such increase would reduce the strain factor and hence the longitudinal partial shear interaction.

A significant drop in strain factor implies that the strain in the steel plate is much lower than the strain in the adjacent concrete, at the centroidal level of the steel plate. The strain reduction in the steel plates reduces the chance of plate yielding, and can greatly reduce the moment capacity of the strengthened beam, as described in Section 3.1. The low chance of plate yielding at the peak moment implies that assuming the steel plates to be plastic at the ultimate state, as adopted in rigid plastic analysis, is not always true in BSP beams, and the strength of the BSP beams can be significantly over-estimated if the steel plate is assumed to be plastic. This suggests that in the ultimate load analysis of BSP beams, the strain reduction in the steel plate should be considered.

The variation of strain factor in specimens can be explained if the relative stiffness between the connecting media and the steel plate in the axial direction is considered. As expected, using more bolts has a positive effect on the longitudinal partial interaction of BSP beams. By comparing Specimens SBWP and WBWP, as well as Specimens WBSP and SBSP, it can be seen that the strain factor increases with the number of bolts used. When more bolts are used, the stiffness of the connecting media is increased, implying that a smaller slip of bolts is required to transfer axial force to

the steel plates. Thus the slip strain, as well as the denominator of the expressions for strain factor in Equation (4), will be decreased, resulting in a larger strain factor.

Meanwhile, from comparing the strain factors of Specimens WBSP and WBWP, it can be observed that the strain factor decreases as the axial stiffness of the steel plates increases. When steel plates of higher axial stiffness are used, a greater axial force will be induced in the plates and a larger bolt slip is needed to transfer the larger axial force to the steel plates. As a result, a larger slip strain will be present at the section considered and the strain factor will be increased accordingly, from Equation (4).

From the above findings, it can be concluded that longitudinal partial interaction of a BSP beam is dependent on the stiffness of the connecting media. The partial interaction increases when the stiffness of connecting media and steel plate increases. A proper selection of bolt-plate arrangements is of utmost importance for the design of BSP beams. Kinematic hardening approach developed by the authors may be used for the analysis of non-linear responses of bolt groups [11].

4.2.2 Curvature factor responses

The curvatures of the RC beam and steel plates were determined from the LVDT and the strain gauge readings, respectively. The curvature factor was solved using Equation (5). Fig. 13 shows the variation of curvature factor against the curvature of the RC beam in the critical moment zone. As shown in Fig. 13, the curvature factors were larger than 0.9 in all specimens prior to yielding of the bottom reinforcement. This means that the difference in curvatures between the RC beam and steel plate at the critical section were small in all specimens and that there was a strong transverse interaction between the RC beam and the steel plates in the elastic stage. Unlike the variation of strain factor in the elastic stage, the curvature remained almost constant

throughout the elastic stage. This suggests that the transverse partial interaction response is less sensitive to the gradual drop in bolt stiffness, as compared with the longitudinal partial interaction response.

After yielding of the bottom reinforcement, the curvature factors began to drop gradually. In the ultimate state, the curvature factors at the critical section of the specimens range from 0.2 to 0.7, which is significant. The reduction in curvature can be explained by the formation of plastic hinges at the critical section. When a plastic hinge forms in the RC beam, the flexural stiffness of the plastic hinge zone drops to almost zero and thus the curvature of the RC beam increases dramatically when being deformed further. On the contrary, due to the reduction of strain in the steel plates, a plastic hinge is unlikely to form in the steel plates, and thus the curvature in the steel plates will not increase as quickly as that of the RC beam. Both effects, together, resulted in the decreasing trend of curvature factor.

For Specimen WBSP, the curvature factor was significantly larger than 1 when the curvature was equal to 0.018 m^{-1}. This is because a large crack was formed on the shear span below the support and the local curvatures near the support were increased rapidly. This effect was unable to be captured by the strain gauges located 600mm away from the supports (see Fig. 5). Hence, the measured average curvature in the RC beam is lower than expected and becomes smaller than the curvature in the steel plates.

The decrease in curvature factor shows that the difference in curvature is more significant as a plastic hinge forms. As one of the governing behaviours affecting the moment resistance of the BSP beam, the effects of a plastic hinge on the difference in curvature should be considered in the ultimate limit state analysis of BSP beams.

4.3 Longitudinal slip profiles

Bolt slips at the specified points on the shear span have been measured by rhombic arrangements of LVDTs. However, such arrangement is not applicable to the constant moment zone. As cracks formed at the bottom face in the constant moment zone, the reference points on the concrete side face would be dislocated, affecting the reliability of the measurement. Thus, the slips in the constant moment zone were revealed by integrating the slip strain between the RC beam and the steel plates, instead of installing additional sets of LVDTs. Further assuming that the slip was zero at mid-span and uniformly varying, the slip in the constant moment zone could be expressed as

$$s_l(x) = (L - x)(\varepsilon_{c,h_p} - \varepsilon_{p,h_p}) \tag{5}$$

where ε_{c,h_p} and ε_{p,h_p} are the strains of concrete and plate, respectively, at the centroidal level of the plate, L and x are half of the clear span and the distance from the support, respectively. The strain of the RC beam at the centroidal level of the plate was estimated by the strain gauges attached on the top and bottom reinforcement. Assuming that plane sections remain planar after bending, the longitudinal strains of the RC beam at the centroidal level of the plate in the constant moment zone were estimated by linear interpolation. On the other hand, the strains of steel plates at the centroidal levels of the plates could be read directly from the strain gauge attached at the corresponding level.

The longitudinal slip responses along the beam span of all strengthened specimens at different load levels are plotted in Fig. 14. When M=0.5M_u, all specimens were elastic and the longitudinal slip profiles were smooth, as illustrated by the dotted lines in Fig. 14. The longitudinal slip was maximal at the supported ends and decreased gradually until reaching zero at mid-span.

As a plastic hinge gradually formed below the loading point, the beam response became non-linear. The plastic hinge zones of specimens are approximated as a segment 200 mm long below the loading point, as illustrated by the dashed line in Fig. 14. According to Fig. 14, there is an abrupt change in longitudinal slip within the plastic hinge zone, equivalent to 42% to 90% of the total change in longitudinal slip for the whole span. The slip strain (the first derivative of the longitudinal slip with respect to the coordinate along the beam) is accumulated in the plastic hinges but not for the remaining parts of the beam. This means that the strain separation between the RC beam and the steel plates is greatest in the plastic hinge, and such effects become greater as the beam gradually approaches its ultimate state. Such an increase in strain separation in the plastic hinge reduces the tensile strain in the steel plates and eventually lowers the flexural strength of BSP beams.

5. Conclusions

The test results of five simply-supported BSP beams with different bolt-plate arrangements have been presented. It is concluded that the formation of plastic hinges in RC core of BSP beams decreases both the longitudinal and transverse partial interactions between the RC beam and steel plates. By introducing deformation-based parameters, i.e. the strain factor and the curvature factor, the degree of interaction between the RC beam and the steel plates is quantified. It was observed that the degree of interaction was reduced by up to 50% as the beam changed from elastic stage to inelastic stage, leading to significant strength reductions since part of the steel plates remained un-yield at ultimate stage. The strength reduction of specimens with full shear connection, in terms of percentage reduction of the increase in flexural strength, varied from 25% to 38%, which is much larger than the 15% allowance

suggested previously by Oehlers et al. [4] and should be heeded when designing BSP beams in practice. The under-estimation of the effect of partial interaction in composite structures could lead to unsafe design. Such effect on the peak and post-peak loading stages warrants further investigations.

Acknowledgements

The research described here was supported by the Research Grants Council of the Hong Kong SAR (Project No. HKU7166/08E). The generous provision of the anchor bolts by the HILTI Corporation is also gratefully acknowledged.

Appendix A

Consider an example when a coordinate system (x,y) is set on the side face of the RC beam. The steel plate slips relatively to the RC beam with an amount (s_l,s_v,s_θ), as illustrated in Fig. A1. The reference points of the steel plate on the metal strip move rigidly together with the target plane of the steel plate. The distances between the reference points are changed and measured by the LVDTs. By doing so, the magnitude of slips could be solved using trigonometry.

The slips at points on the shear span are measured by rhombic arrangements of LVDTs. The LVDTs measure relative movements between reference points as load is applied to the beams. The original length of the LVDT set (L_{LVDT}) is equal to the initial distance between the reference points on the RC and steel plate, which can be expressed as

$$L_{LVDT} = \frac{\sqrt{L_{rs}{}^2 + L_{rc}{}^2}}{2} \tag{A1}$$

where L_{rs} and L_{rc} are the distances between the reference points on the steel plate and reinforced concrete, respectively. The instantaneous distances between the reference points *ab*, *bd*, *ac* and *cd* could be expressed as

$$l_{ab} = L_{LVDT} + \Delta l_{ab}\,, \tag{A2}$$

$$l_{bd} = L_{LVDT} + \Delta l_{bd}\,, \tag{A3}$$

$$l_{ac} = L_{LVDT} + \Delta l_{ac}\,, \tag{A4}$$

$$l_{cd} = L_{LVDT} + \Delta l_{cd}\,, \tag{A5}$$

where $\Delta l_{ab}, \Delta l_{bd}, \Delta l_{ac}, \Delta l_{cd}$ are the readings of LVDTs between the nodes denoted by the subscripts.

Using trigonometric relationships, the slip in different directions could be expressed as

$$s_x = -\left(L_{LVDT} + \Delta l_{ab}\right)\sin\lambda + \frac{L_{rs}}{2}\sin\left(\lambda + \delta\right) \tag{A6}$$

$$s_y = \frac{L_{rc}}{2} - \left(L_{LVDT} + \Delta l_{ab}\right)\cos\lambda + \frac{L_{rs}}{2}\cos\left(\lambda + \delta\right) \tag{A7}$$

$$s_\theta = \frac{\pi}{2} - \lambda - \delta \tag{A8}$$

where $\lambda = \cos^{-1}\left(\dfrac{{L_{rc}}^2 + {l_{ab}}^2 - {l_{bd}}^2}{2 l_{ab} L_{rc}}\right)$ and $\delta = \cos^{-1}\left(\dfrac{{L_{rs}}^2 + {l_{ab}}^2 - {l_{ac}}^2}{2 l_{ab} L_{rs}}\right)$.

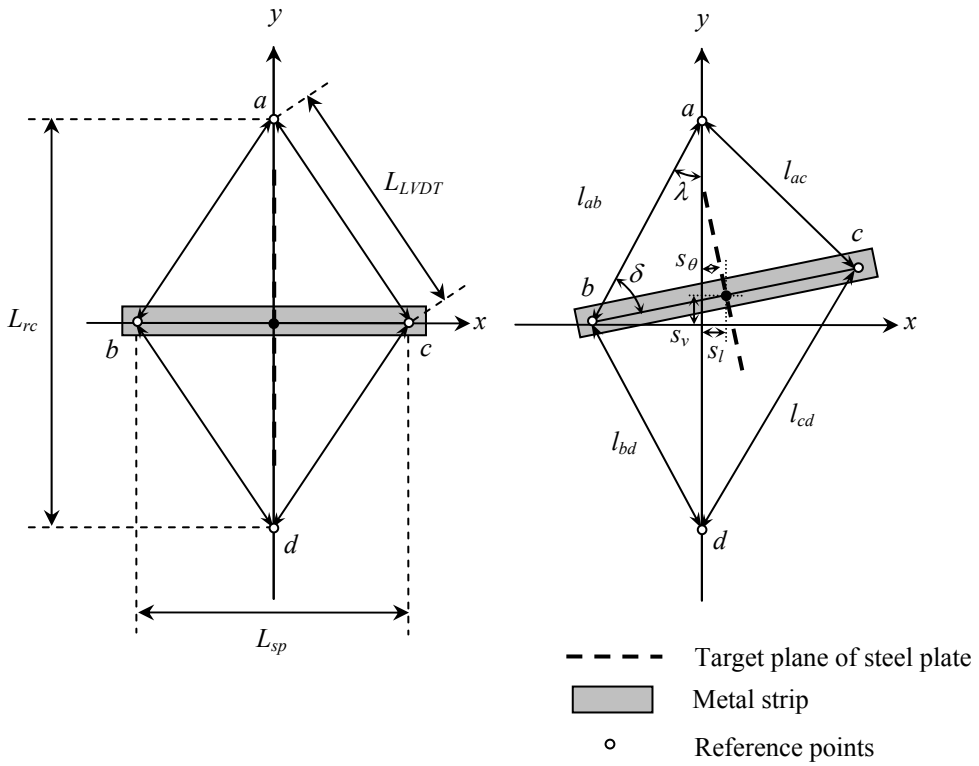

Fig. A1. Schematic diagram of rhombic arrangement of LVDTs in motion

Appendix B

The concrete model used was based on the model proposed by Attard and Stewart [7], with minor modifications to account for the local properties of concrete. In the proposed model, the parameters required are the initial Young's modulus of concrete E_c, the peak compressive stress of concrete f_{co} and the corresponding strain ε_{co}, and the stress f_{ci} and strain ε_{ci} of the inflection point on the descending branch of the model. The compressive stress of concrete σ_c can be related to the compressive strain ε_c by

$$\sigma_c / f_{co} = \frac{A(\varepsilon_c / \varepsilon_{co}) + B(\varepsilon_c / \varepsilon_{co})^2}{1 + (A-2)(\varepsilon_c / \varepsilon_{co}) + (B+1)(\varepsilon_c / \varepsilon_{co})^2} \tag{B1}$$

where

$$A = \frac{E_c \varepsilon_{co}}{f_{co}}; \quad B = \frac{(A-1)^2}{0.55} - 1 \quad \text{for} \quad \varepsilon_c \le \varepsilon_{co} \tag{B2}$$

$$A = \frac{f_{ci}(\varepsilon_{ci} - \varepsilon_{co})^2}{\varepsilon_{co}\varepsilon_{ci}(f_{co} - f_{ci})}; \quad B = 0 \quad \text{for} \quad \varepsilon_c > \varepsilon_{co} \tag{B3}$$

To account for local properties of concrete, the following relationships, expressing the parameters E_c, ε_{co}, f_{ci}, ε_{ci} in terms of f_{co} [8], were adopted in this study.

$$E_c = 7200(f_{cu})^{1/3} \cong 7200(1.25 f_{co})^{1/3} \tag{B4}$$

$$\varepsilon_{co} = 700(f_{co} / E_c)^2 - 2.8(f_{co} / E_c) + 0.0059 \tag{B5}$$

$$f_{ci} / f_{co} = 1.77 - 0.4 \ln(f_{co}) \tag{B6}$$

$$\varepsilon_{ci} / \varepsilon_{co} = 3.86 - 0.54 \ln(f_{co}) \tag{B7}$$

The peak compressive stress f_{co} is actually the *in situ* uniaxial compressive strength of concrete, which can be determined from the cylinder compressive strength f_c or modified from the cube compressive strength by applying a suitable conversion factor.

References

[1] Oehlers DJ, Nguyen NT, Ahmed M, Bradford MA. Transverse and longitudinal partial interaction in composite bolted side-plated reinforce-concrete beams. Structural Engineering and Mechanics 1997;5(5):553-564

[2] Nguyen NT, Oehlers DJ, Bradford MA. An analytical model for reinforced concrete beams with bolted side plates accounting for longitudinal and transverse partial interaction. International Journal of Solids and Structures 2001:38;6985-6996

[3] Ahmed M, Oehlers DJ, Bradford MA. Retrofitting reinforced concrete beams by bolting steel plates to their sides. Part 1: Behaviour and experimental work. Structural Engineering and Mechanics 2000;10(3):211-226

[4] Oehlers DJ, Ahmed M, Bradford MA, Nguyen NT. Retrofitting reinforced concrete beams by bolting steel plates to their sides. Part 2: Transverse interaction and rigid plastic design. Structural Engineering and Mechanics 2000;10(3):227-243

[5] Su RKL, Siu WH and Smith ST, Effects of bolt-plate arrangements on steel plate strengthened reinforced concrete beams. Engineering Structures (Submitted in April 2009)

[6] Fastening technology manual, Issue 2005/06, Hilti Corporation.

[7] Attard, MM, Stewart, MG, A two parameter stress block for high strength concrete, ACI Structural Journal 1998; 95(3): 305-317.

[8] Su RKL, Cheng B, The effect of coarse aggregate size on the stress-strain curves of concrete under uniaxial compression, Transactions of Hong Kong Institution of Engineers 2008, 15(3): 33-39

[9] Siu WH and Su RKL, Nonlinear analysis of bolted side-plated reinforced concrete beams, Proceedings of the First International Conference on Computational Technologies in Concrete Structures, 24-27 May 2009, Jeju, Korea, 667-679.

[10] Siu WH and Su RKL, Analysis of side-plated reinforced concrete beams with partial interaction, Computers and concrete (Accepted in July 2009).

[11] Siu WH and Su RKL, Load-deformation prediction for eccentrically loaded bolt groups by a kinematic hardening approach, Journal of Constructional Steel Research 2009, 65(2): 436-442.

Table 1. Summary of bolt-plate arrangements of BSP specimens

	Specimen SBSP	Specimen WBSP	Specimen WBWP	Specimen SBWP
No. of bolts on shear span#	8	3	3	5
Plastic strength of bolts on a shear span P_b (kN)	608	228	228	380
Plate size# (mm×mm)	6×150dp.	6×150dp.	6×75dp.	6×75dp.
Maximum plate force from full interaction analysis $F_{p,fi}$ (kN)	605	605	302	302
Degree of shear connection η	1.00	0.38	0.75	1.26
Concrete cube strength (MPa)	34.6	34.3	35.1	35.3

#value refers to the plate on each face of the beam

Table 2. Material properties of reinforcement and steel plates

Material properties	Reinforcement		Steel plate	
	T-10	T-16	75mm (deep)	150mm (deep)
Yield Strength (MPa)	545	537	338	335
Young's Modulus (GPa)	190	187	203	212
Yield Strain	0.00287	0.00287	0.00167	0.00159

Table 3. Strength and failure modes of specimens

Specimen	Failure mode	M_u (kNm)	Increase in strength (%)
NBNP	Concrete Crushing	101.4	-
SBSP	Concrete Crushing	161.5	59
WBSP	Bolt fracture	149.2	47
WBWP	Bolt fracture	133.4	32
SBWP	Concrete Crushing	144.6	43

Table 4. Bolt slip at peak load

Specimen	200mm from support	1000mm from support	Bolt failed
SBSP	1.2	0.9	No
WBSP	4.6	3.8	Yes
WBWP	4.2	4.0	Yes
SBWP[#]	1.7	1.6	No

The locations where measurements were made were at 175mm and 1025mm from support

Table 5. Summary of strengthening performance of BSP beams

		NBNP	SBSP	WBSP	WBWP	SBWP
Degree of shear connection η		N.A	1.00	0.38	0.75	1.26
From the present tests	Ultimate moment M_u (kNm)	101.4	161.5	149.2	133.4	144.6
	Additional moment ΔM_u (kNm)	-	60.1	47.8	32.0	43.2
From full-shear-connection full-interaction analysis	Ultimate moment $M_{u,fsc,fi}$ (kNm)	95.9	193.5	193.5	153.3	153.3
	Additional moment $\Delta M_{u,fsc,fi}$ (kNm)	-	97.6	97.6	57.4	57.4
$\Delta M_u/\Delta M_{u,fsc,fi}$		-	0.62	0.49	0.56	0.75
Reduction in the increase in moment resistance (%)		-	38	51	44	25

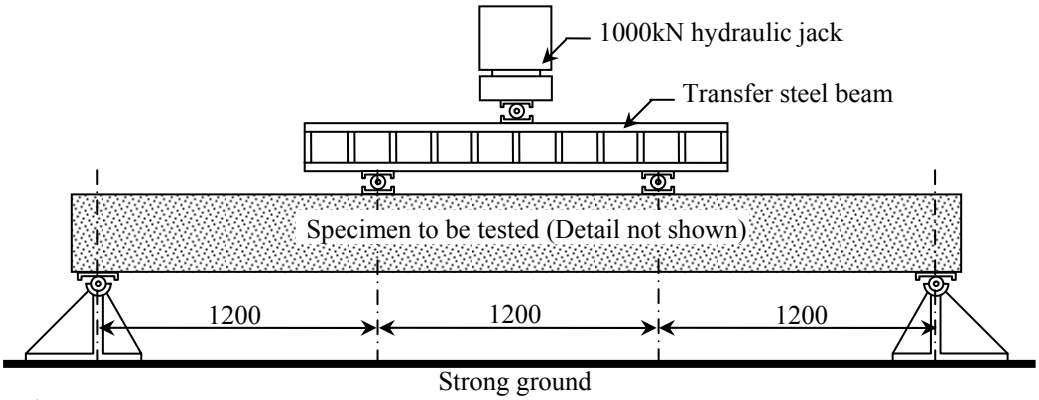

a)

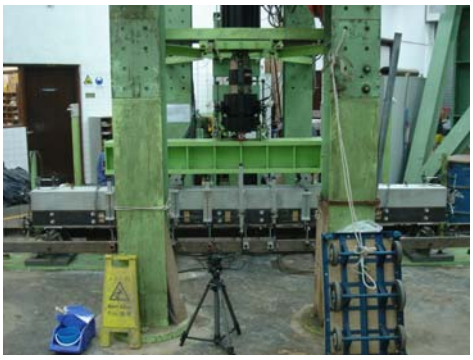

b)

Fig. 1. Test setup a) Schematic diagram, and b) Actual arrangement

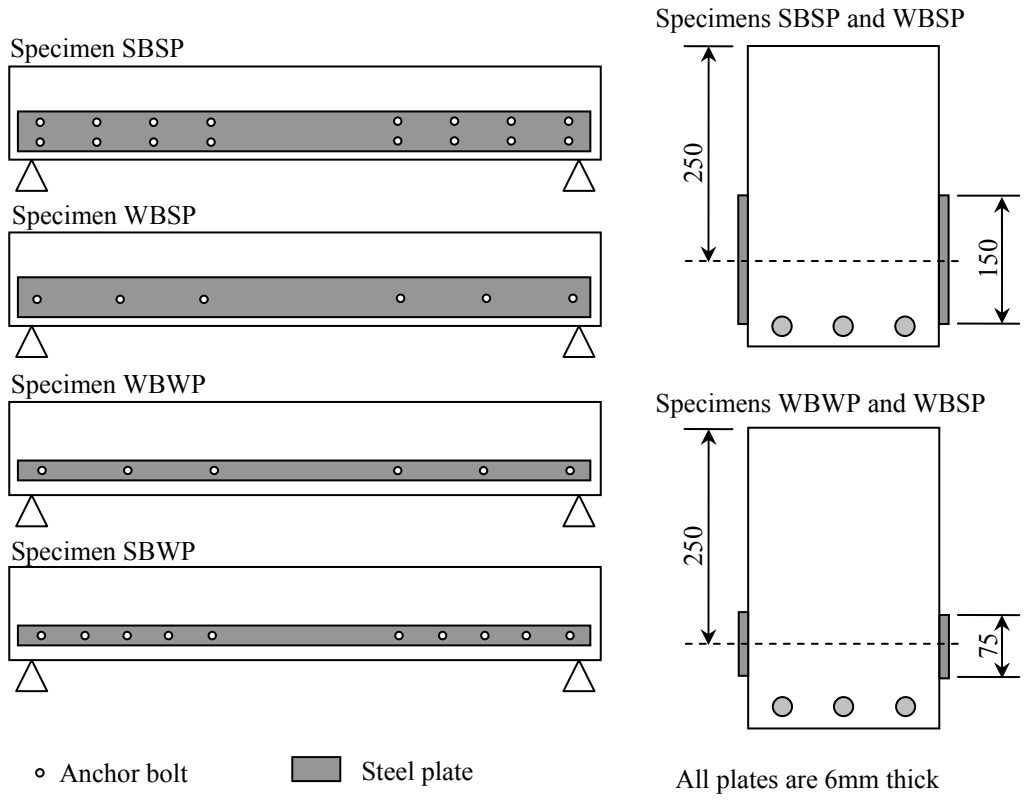

Fig. 2. Bolt-plate arrangements of BSP specimens

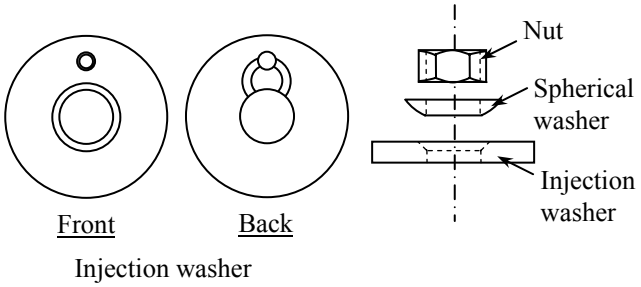

Fig. 3. Diagrammatic illustration of a dynamic set washer

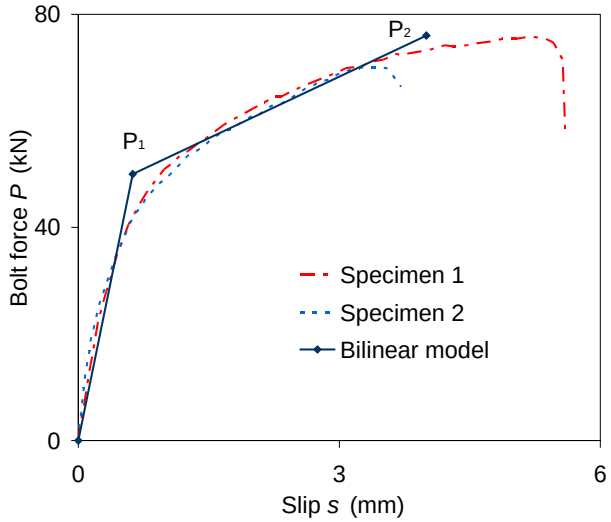

Point	s (mm)	P (kN)
P_1	0.625	50
P_2	4.0	76

Fig. 4. The load-slip relationship of anchor bolts

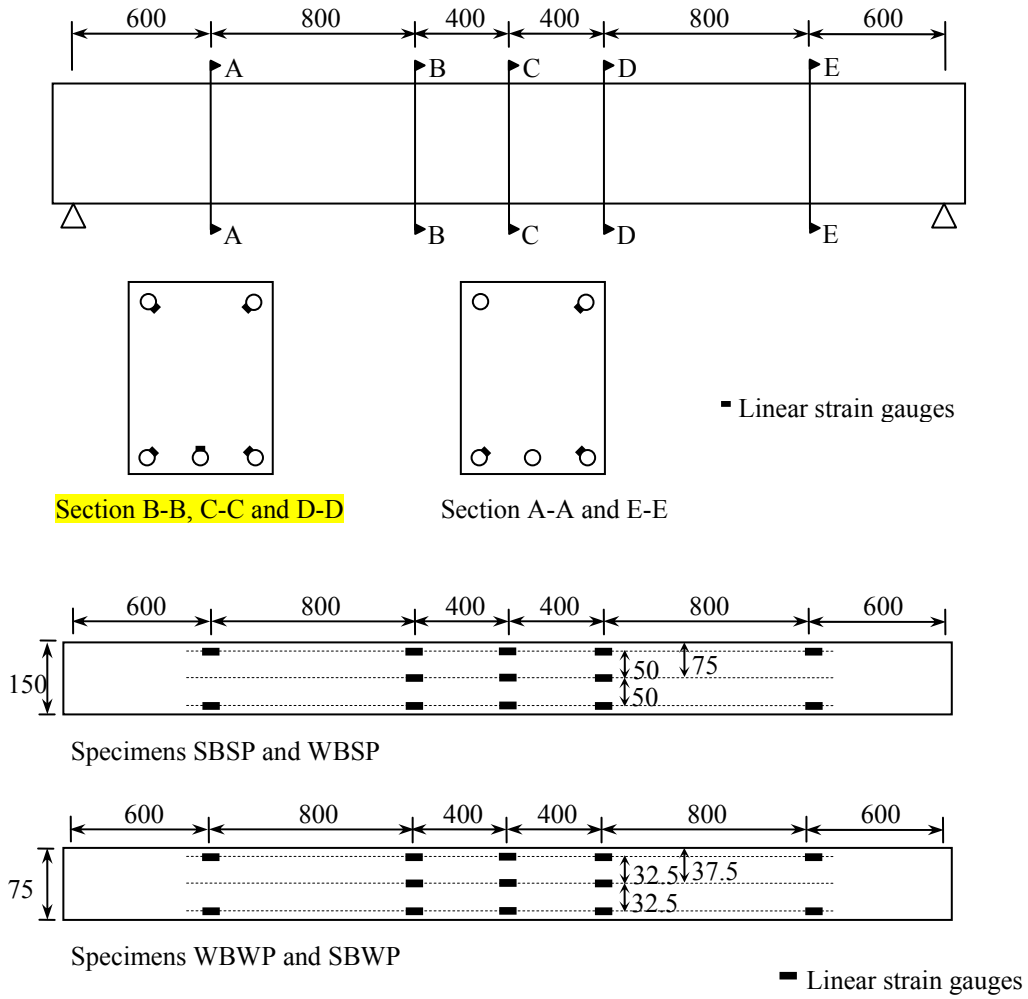

Fig. 5. Strain gauges attached on the reinforcement and the steel plates

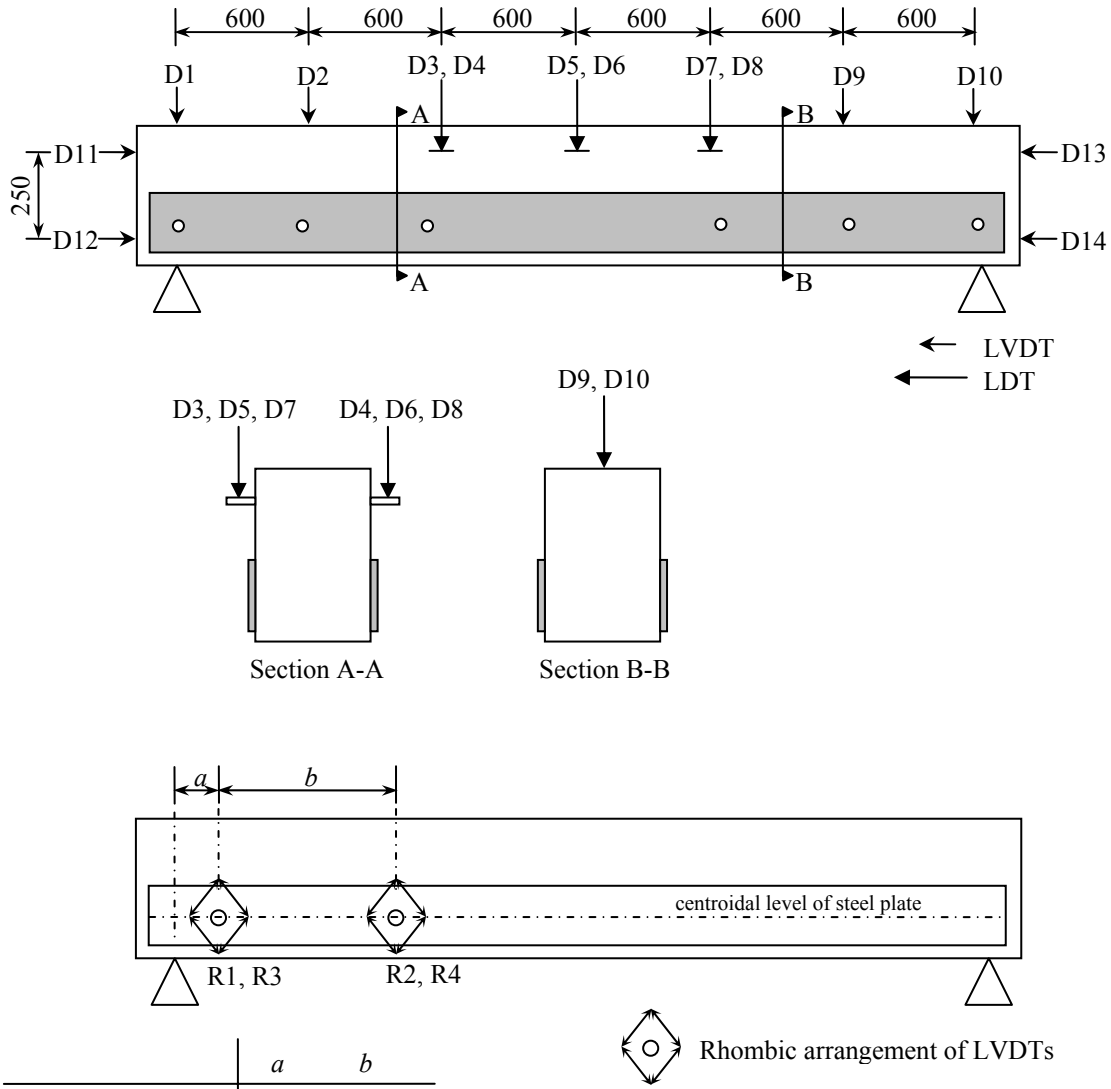

	a	*b*
Specimens SBSP, WBSP and WBWP	200	800
Specimen SBWP	175	850

Fig. 6. LVDT and LDT arrangements for the specimens

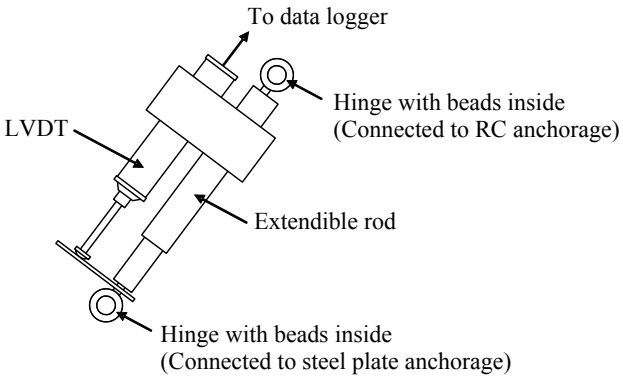

(a)

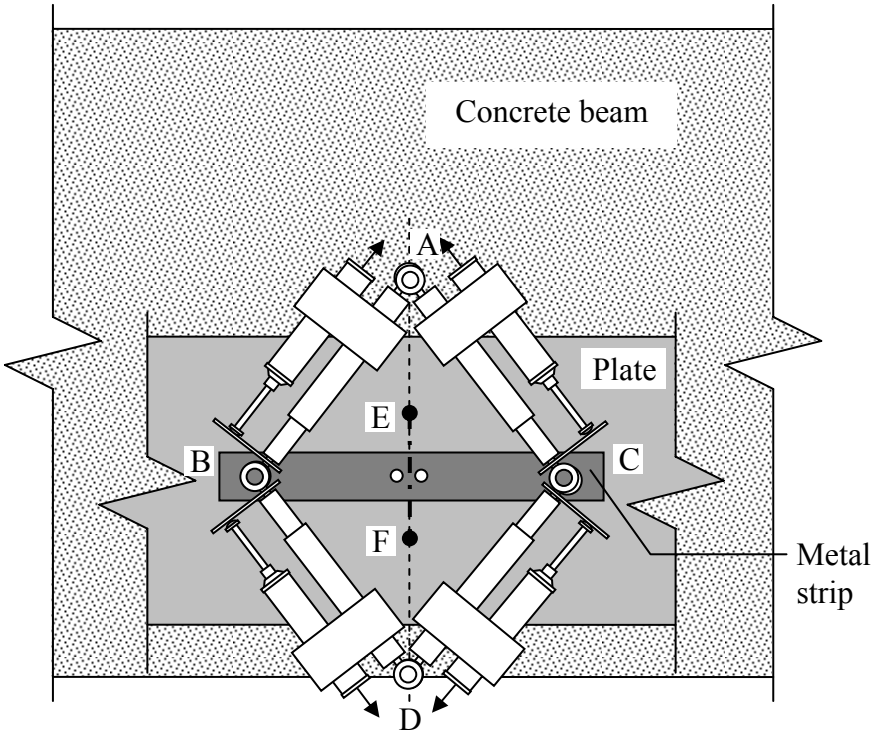

(b)

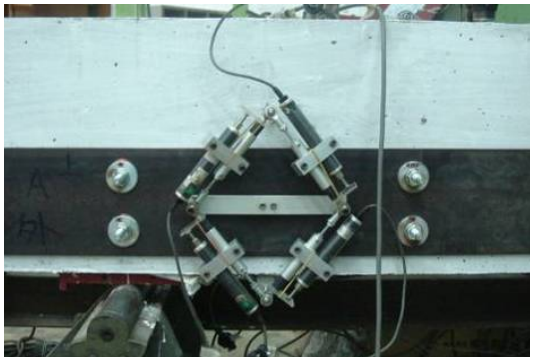

(c)

Fig. 7. Schematic arrangement of rhombic set of LVDTs (a) setup of a LVDT (b) setup of a group of LVDTs, and (c) Actual arrangement

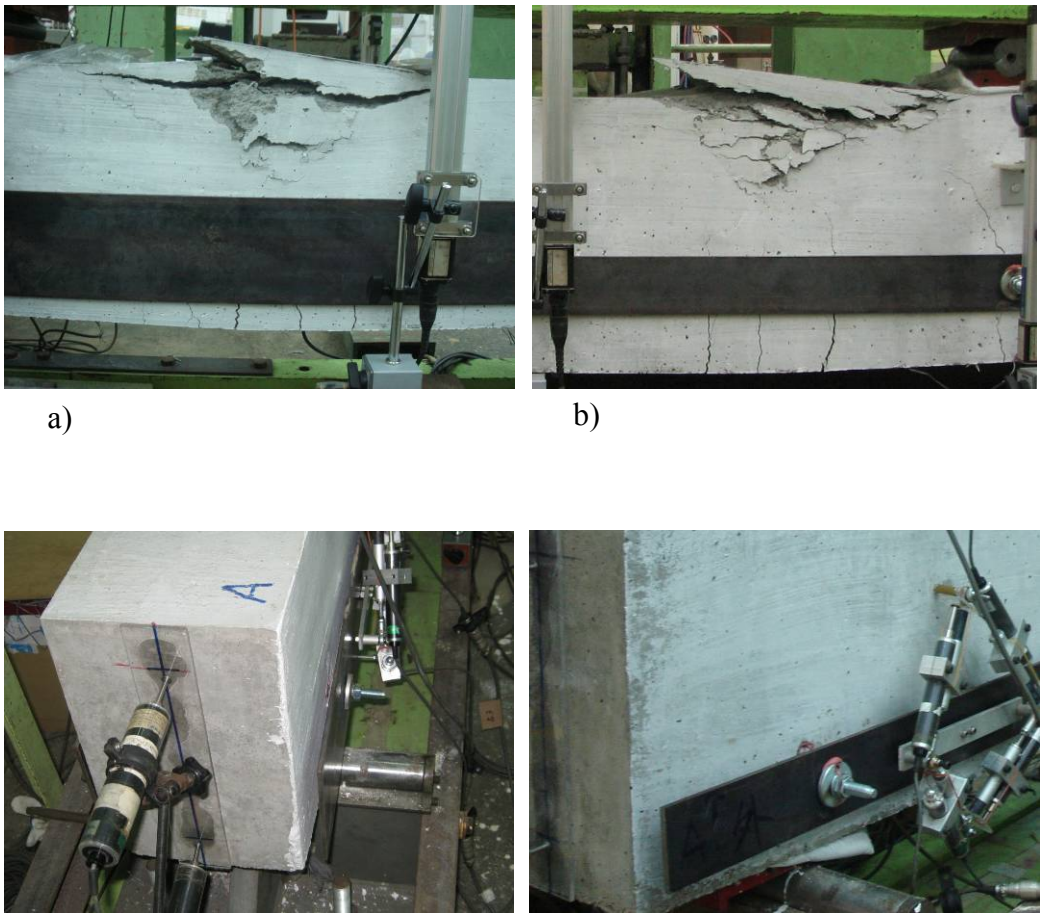

Fig. 8. Failure modes of specimens (a) SBSP, (b) SBWP, (c) WBSP, and (d) WBWP

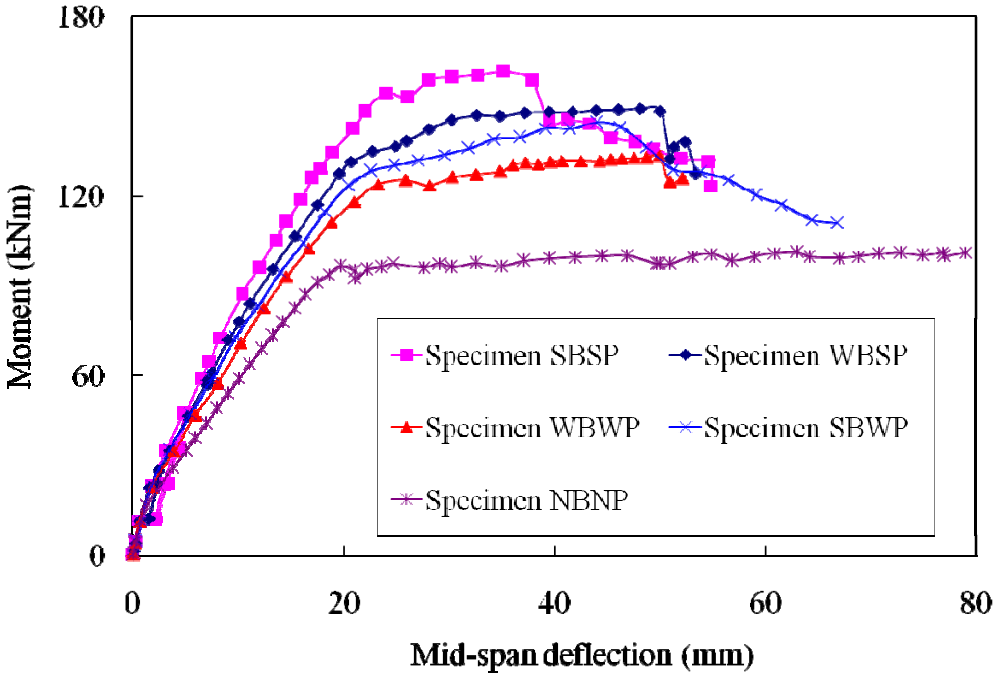

Fig. 9. Moment-deflection curves of specimens

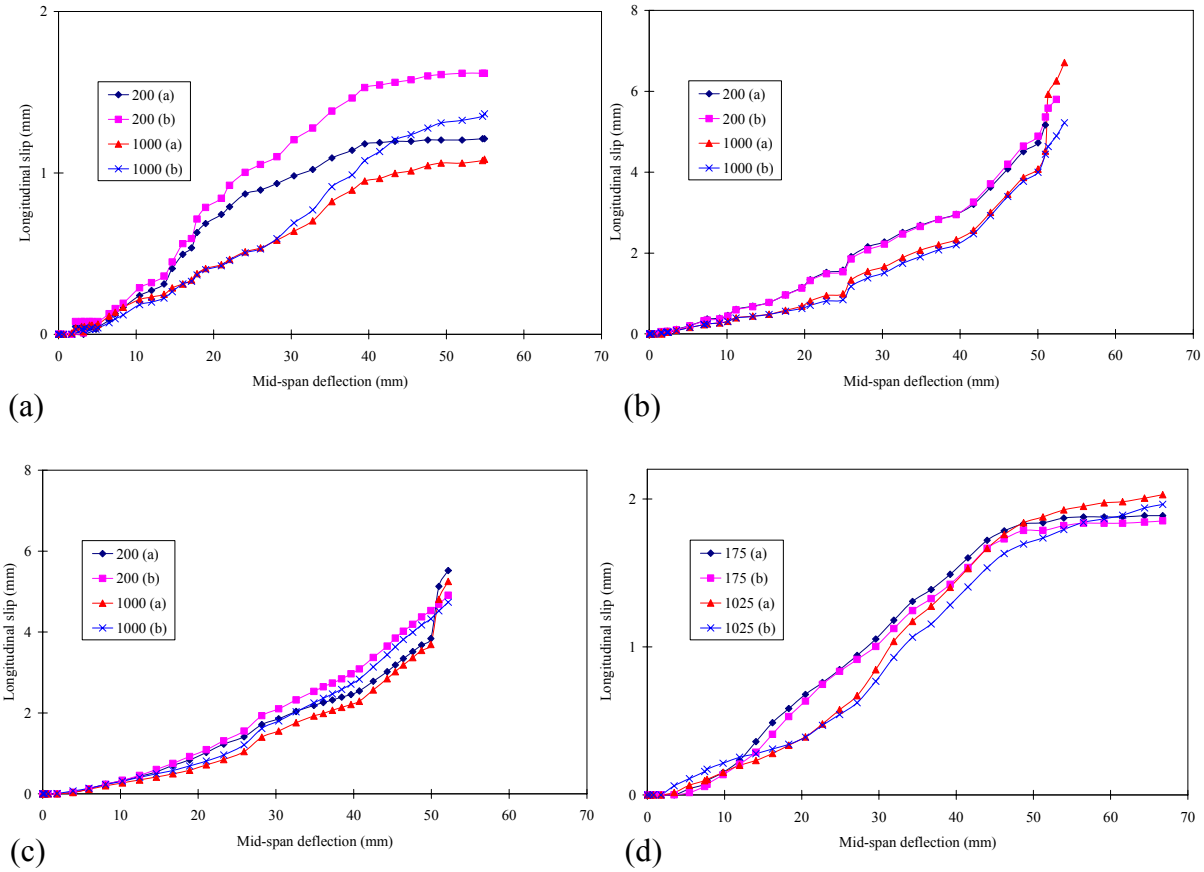

Fig. 10. Longitudinal slip responses against mid-span deflection (a) Specimen SBSP, (b) Specimen WBSP, (c) Specimen WBWP, and (d) Specimen SBWP

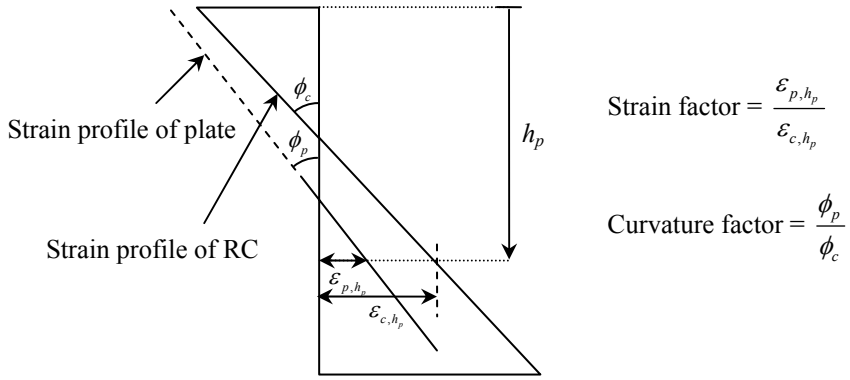

Fig. 11. Definitions of strain factor and curvature factor (at the section subjected to the peak moment)

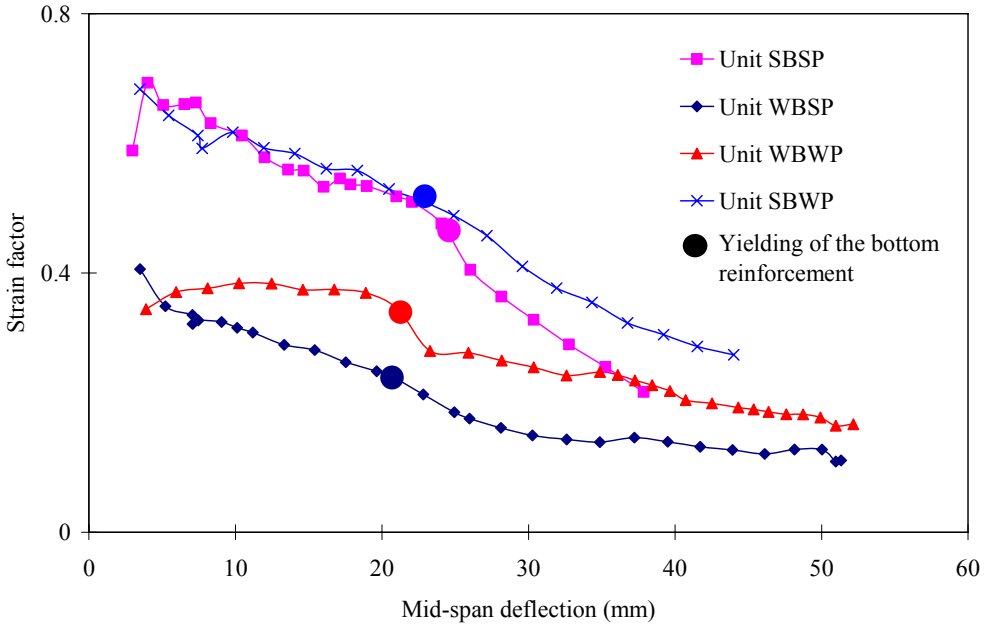

Fig. 12. Variations of strain factor with the mid-span deflection of RC beam

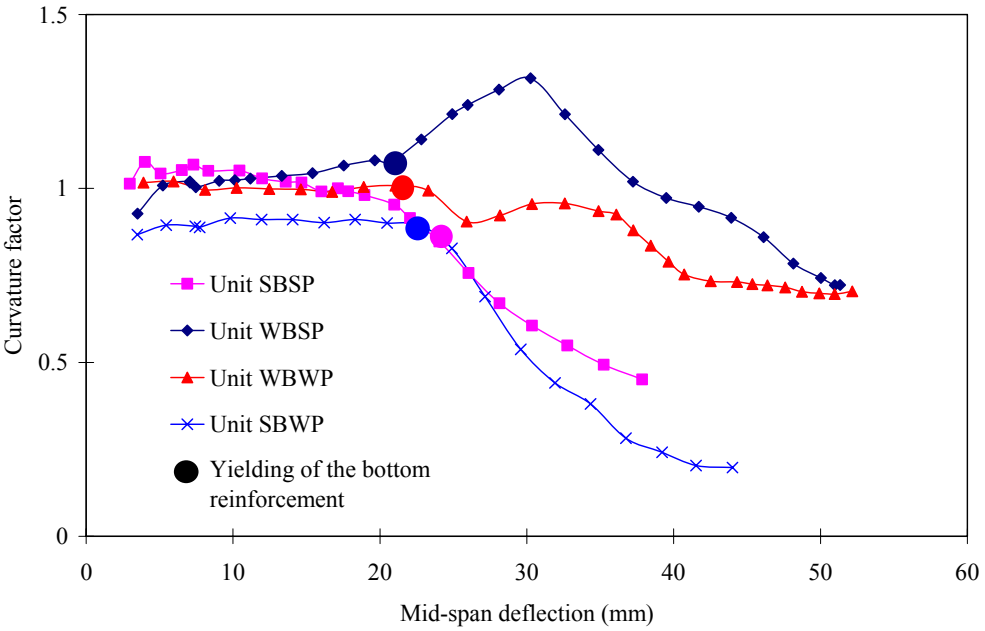

Fig. 13. Variations of curvature factor with the mid-span deflection of RC beam

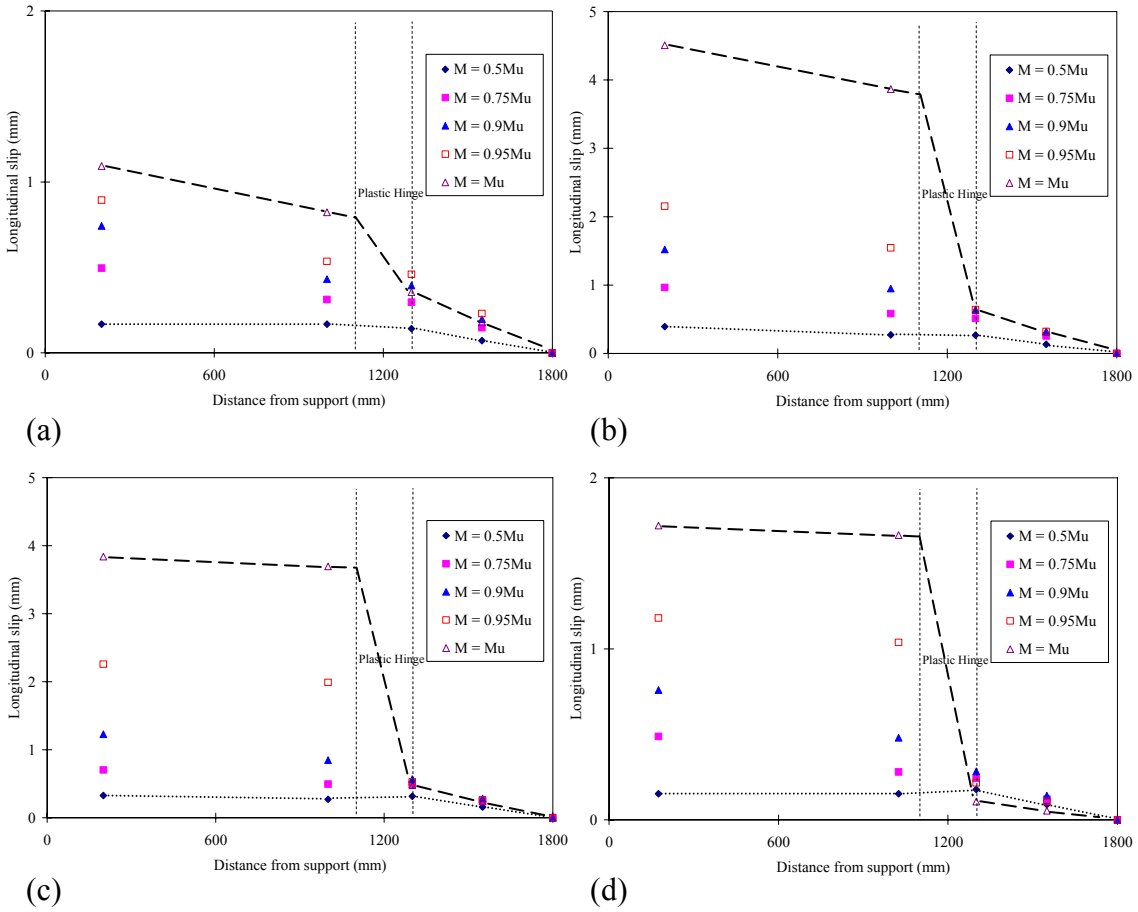

Fig. 14. Longitudinal slip responses along beam spans (a) Specimen SBSP, (b) Specimen WBSP, (c) Specimen WBWP, and (d) Specimen SBWP